Applied Mathematics & Information Sciences
An International Journal

http://dx.doi.org/10.18576/amis/190108

Nonlinear Autoregressive Neural Network with Exogenous Input Model Approach for Magnetic Flux Density Measured by Hall-Effect Sensor in Magnetic Spring

Grazia Lo Sciuto [1,*], *Joanna Bijak* [1], *Zygmunt Kowalik* [1], *Tomasz Trawiński* [1], *Nadir Omer* [2] *and Mohammed Sallah* [3]

[1]Department of Mechatronic, Faculty of Electrical Engineering, Silesian University of Technology, Akademicka 10A, Gliwice, 44-100, Poland
[2]Department of Information Systems, College of Computing and Information Technology, University of Bisha, Bisha, 61922, Saudi Arabia
[3]Applied Mathematical Physics Research Group, Physics Department, Faculty of Science, Mansoura University, Mansoura, 35516, Egypt

Received: 31 Jul. 2024, Revised: 26 Sep. 2024, Accepted: 29 Sep. 2024
Published online: 1 Jan. 2025

Abstract: In this study, the magnetic and mechanical properties of the magnetic spring system are investigated. Experimental tests of the levitating magnet displacement in the magnetic spring are conducted by the laser distance meters and the detection of the magnetic flux density in the magnetic spring is provided by the three Hall-effect sensors. The measurements of the displacement and magnetic flux density in the magnetic spring excited by the vibration generator are characterized by nonlinear behaviour. The nonlinear mathematical model is proposed to predict and approximate the magnetic flux density starting from geometrical properties, voltage of vibration generator, frequency and displacement of the levitating magnet based on the nonlinear autoregressive networks with exogenous input (NARX) neural network architecture. The accuracy of the results obtained by NARX emphasises as the modeling technique can be used for construction and design of non-linear magnetic spring devices.

Keywords: Magnetic spring, NARX neural network, energy harvesting, displacement, magnetic flux density, Hall-Effect sensors.

1 Introduction

The renewable energy sources are being explored in response to the reduction of the system operating cost which are related to the environmental protection from fossil fuels pollution and global warming. Energy harvesters (EHs) convert the solar, wave, wind, thermal, biological or kinetic energy to electrical energy [1]. EHs are optimized to ensure the reliable power supply to autonomous or hard-to-reach systems and lower systems usage cost [2, 3]. Kinetic energy derived from the environmental mechanical vibrations is converted to the electrical energy by vibration energy harvesters (VEHs) that mostly operate by means of piezoelectric, electrostatic and electromagnetic transducers. The electromagnetic transducers are commonly used to harvest the vibration from the house appliances, vehicles, buildings or even the human motion [4–8].

Electromagnetic vibration energy harvesters (EMVEHs) are inertial generators designed as a system of a proof-mass (magnet), frame (coil and carcass) and holding mechanism (spring). External vibrations force moves the frame and, in consequence, inertial and potential forces act on a proof-mass. The mechanical external vibrations are converted into electrical energy [9, 10]. In the EMVEH the induced voltage depends on the parameters of the coil, velocity of the proof-mass and the magnetic flux density. The last one is affected by the relative position of the magnet and coil. In EMVEHs the holding mechanisms usually comprise the mechanical spring [11–13]. However, the mechanical springs is limited by fatigue life and by the resonance

* Corresponding author e-mail: grazia.loSciuto@polsl.pl

frequency. Therefore the other solutions are investigated like planar springs with several frequencies and high deformation capability, and magnetic spring with nonlinear spring force [14, 15]. In the magnetic spring, repulsive forces between two magnets provide the nonlinear stiffness of the holding mechanisms with higher life expectancy than traditional springs. In order to enhance the energy, magnetic spring based energy harvester with one fixed and two levitating magnets repelling each others was proposed in [16]. The magnetic flux density distribution and the output power under excitation motion in EMVEHs are investigated by the Finite Element Method (FEM) [16–18]. The motion of the floating magnet caused by the environmental vibration in the EMVEHs depends on the parameters of a spring [19, 20].

In order to improve the efficiency of the energy harvester the optimization is focused on the coil, magnetic field and mechanical properties of the magnetic spring, and performed by mathematical models such as FEM [21, 22]. The prediction of the magnetic field and in consequence also magnetic flux density distribution is conducted by Artificial Neural Networks (ANN) [23, 24]. The authors in [25] proposed 3-D numerical model of the magnetic field based on ANN and the optimization of the coil geometry based on the distribution of the magnetic field can be solved by the ANN according to [26]. The estimation of vibration and its resonance frequency in the EMVEHs can be processed by the ANN combined with optical measurements [20, 27, 28]. The nonlinear dynamics of the magnetic spring based EMVEH enhance the resonance frequency bandwidth and also the harvested power, although the benefits of the combination of the nonlinearity could be considered an issue for the modeling due to the complexity of the magnetic spring device. For instance, the optimization of the energy harvester have been conducted in many studies using different approach such as genetic algorithm and methodology based on artificial intelligence [29–32]. In particular the machine learning algorithm do not request complex mathematical relation between inputs and output parameters.

In this work, the new approach based on neural network is investigated as a solution to overcome issues related to the non-linearity and complexity of the magnetic spring. The measurements of the floating magnet displacement conducted by the laser distance meters and the magnetic flux density detected by the Hall-Effect sensors in the magnetic spring are characterized by the high instability due to the nonlinear vibrations generated by the vibration generator [33, 34]. The nonlinear autoregressive networks with exogenous input (NARX) model has been developed to describe the magnetic flux density dependence on the geometrical, magnetic and electrical parameters of the entire tested system. In the proposed theoretical model, the magnetic flux density is a function of the geometrical parameters of the magnetic spring, input voltage of vibration generator, input voltages frequency and the displacement of the levitating magnet. On the other hand, the prediction of the magnetic flux density in the magnetic spring was estimated using NARX neural network.

The novelty of this research focuses on the description of the relation between the magnetic spring parameters and the magnetic flux density that is useful for the improvement of the magnetic spring to the various applications in energy harvesting systems. This study has demonstrated a good accuracy of the NARX approach for the proposed prediction model applied to the magnetic spring.

The laboratory station in the Department of Mechatronics, Silesian University of Technology, Gliwice, Poland was provided for the measurement tests of the magnetic flux and the displacement in magnetic spring.

In Section 2 the design and description of the realized magnetic spring and vibration generator have been discussed. Next, the experimental setup and measurement test results of the displacement and magnetic flux density are presented in Section 3. Subsequently, the architecture and model of the neural network have been designed in Section 4. Finally a conclusion has been reported in Section 5.

2 Design and work principles of the magnetic spring and vibration generator

The magnetic spring investigated in the Laboratory of the Department of Mechatronics, Silesian University of Technology is realized as a set of magnets that repel each other. The magnetic spring prototype consists of two identical neodymium fixed magnets and one neodymium levitating magnet located between them as shown in Fig. 1 (a). The fixed magnets have the cylindrical shapes with both, diameter and height, of 5 *mm* (N38 f). The levitating magnet is also cylindrical with diameter of 10 *mm* and height of 3 *mm* (N38 l) (Fig. 1 (b)).

Table 1: Magnetic properties of material.

Type	m [g]	Br [T]	HcB [kA/m] (min.)	HcJ [kA/m] (min.)
N38 f	0.74	1.21 - 1.25	899	955
N38 l	1.77	1.21 - 1.25	899	955
F30	192.76	min. 0.37	175	180

In the manufactured magnetic spring, the fixed magnets are placed 4 *mm* from levitating magnet. Parameters of the magnets: weight (m), remanence (Br) and coercivities (HcB and HcJ) are presented in the table 1.

The position of the levitating magnet changes during the motion of the magnetic spring provided by external vibrations. In this research the magnetic spring was moved by the vibration generator.

The magnetic spring is enclosed in the polyamide cylindrical casing with two thread fastening elements that arranged the fixed magnets. The casing has a vertical gap that acts as a vent to reduce inside the air pressure.

The repulsive force between two magnets is presented by the equation formula [35]:

$$F_z = \frac{J_1 J_2}{2\mu_0} \sum_{i=1}^{2} \sum_{j=3}^{4} (-1)^{i+j} a_1 a_2 a_3 f_z \tag{1}$$

where J_1 and J_2 are magnetization (polarization) of the magnets along z direction, μ_0 is the magnetic permeability of free space, a_1, a_2 and a_3 are geometrical parameters as reported in [35] and f_z is defined as:

$$\begin{aligned} f_z = K(a_4) - \frac{1}{a_2} E(a_4) + \\ + \left(\frac{a_1^2}{a_3^2} - 1 \right) \Pi \left(\frac{a_4}{1 - a_2} | a_4 \right) \end{aligned} \tag{2}$$

where K, E and Π are complete elliptic integrals of first, second and third kind respectively. The geometrical parameters are defined as:

$$\begin{aligned} a_1 = z_i - z_j; a_2 = \frac{(r_1 - r_2)^2}{a_1^2} + 1; \\ a_3 = \sqrt{(r_1 + r_2)^2 + a_1^2}; a_4 = \frac{4 r_1 r_2}{a_3^2} \end{aligned} \tag{3}$$

where z_i and z_j are displacements of the centers of the magnets along z axis, for first magnet the displacements are z_1 and z_2, for second magnet the displacements are z_3 and z_4, and the radii of first and second magnet are r_1 and r_2 respectively.

In the magnetic spring there are two identical repulsive forces between the levitating and fixed magnets considered nonlinear spring forces. The force acting on the levitating magnet is the sum of these repulsive forces that rely on the geometrical and magnetic parameters of magnetic spring, magnetic flux density of the magnets and the displacement of the magnet. The stiffness of the magnetic spring is derived by differential of the magnetic spring force and is nonlinear depending on the displacement of the levitating magnet in the magnetic spring. The resonance frequency of the magnetic spring is function of the stiffness, as shown in Eq.4.

$$f_0 = \frac{1}{2\pi} \sqrt{\frac{k_s(z_m)}{m_l}} \tag{4}$$

where k_s is the vertical stiffness coefficient of the magnetic spring, z_m is the levitating magnet displacement in the magnetic spring and m_l is the mass of the levitating magnet.

Moreover a strong correlation between the magnetic flux density and displacement of the levitating magnet appears in the magnetic spring. The displacement of the levitating magnet is mostly linear. However, the non-uniform magnetization of the magnets lead to imbalance of forces acting on the levitating magnets causing its rotational movement around the axis perpendicular to the main axis of.

The magnetic spring is standing up on vibration generator for this reason the gravitational force acts on the levitating magnet with effect of the small initial deflection of magnetic spring, as shown in Figure 2

The vibration generator is the vibration source for the magnetic spring. The motion of the magnetic spring depends on the external vibrations that affect the displacement of the levitating magnet and the magnetic flux density. The vibration generator realized in Laboratory of Department of Mechatronics, Silesian University of Technology, Gliwice consists of the electromagnetic cylindrical copper coil wounded in the aluminium carcass on the rod, the ring permanent sintered ferrite magnet placed between two steel fastening ring, the steel magnetic core and two beryllium bronze planar springs (Figure 3(a)). The electromagnetic device generates vibrations at the application of AC voltage to the coil that is converted into varying magnetic field. In consequence the Lorentz force acts on the coil causing its movement. The aluminium casing of the vibration generator is 6 *cm* height with diameter of 10 *cm* and it is used as an insulator for the magnetic field of the permanent magnet. The coil has 280 number of turns, inner and outer radius of 17.5 *mm* and 19.5 *mm* respectively.

The wire of which the coils is wounded has diameter of 0.3 *mm* and length of 32.5 *mm*. The permanent magnet and the fastening rings have outer and inner diameter of 80 *mm* and 40 *mm* respectively. The permanent magnet is 12 *mm* height and is made of barium ferrite ($BaFe12O19$) and strontium ferrite ($SrFe12O19$), and its parameters are presented in the Table 1 (F30 D80 X D40 X 12). The fastening rings are 7 *mm* and 10 *mm* height. The magnetic core is properly shaped to ensure the optimal magnetic flux distribution in the vibration generator (Figure 3 (b)).

The planar springs are 0.3 *mm* thick and are attached to the casing on the bottom and upper part of the vibration generator. Their shape composed by several planar beams ensures few resonance vibration frequencies generated by the vibration generator. In our case, the resonance frequencies for the realized vibration generator (f_{g0}) are $\sim$ 2 *Hz*, 30 *Hz*, 50 *Hz* and 70 *Hz*. The vibrations amplitude of the vibration generator is limited by the strength of the planar springs.

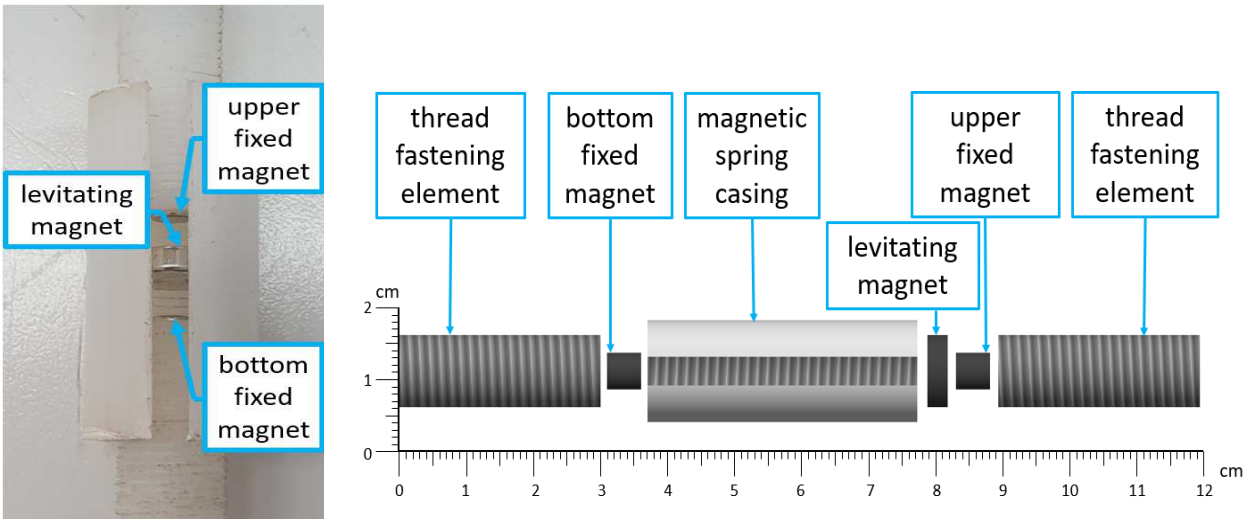

(a) (b)

Fig. 1: (a) Prototype of magnetic spring; (b)Structure of the magnetic spring

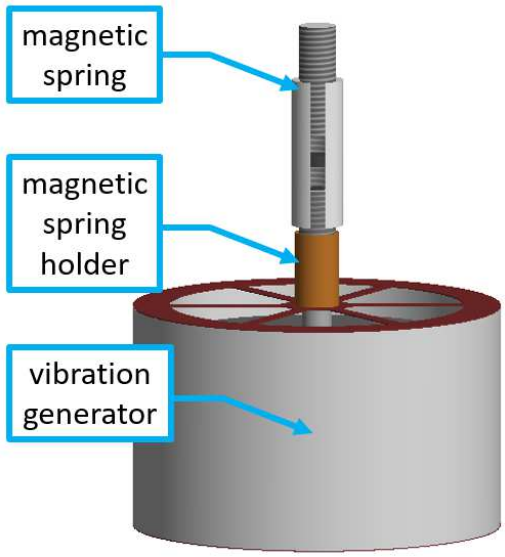

Fig. 2: Magnetic spring on the vibration generator.

3 Experimental results and discussion

3.1 Laboratory setup for measurements of displacement and magnetic flux density

In this research scientific activity, the measurements of magnetic flux density in magnetic spring and magnetic spring's displacement induced by the external vibration have been conducted. The motion of the magnetic spring, due to the vibration, generated by vibration generator, causes displacement of the levitating magnet that affects the magnetic flux density. Hence the Laboratory Stand was provided to measure the displacement and magnetic flux density in the magnetic spring.

The Laboratory stand was equipped by Hall-Effect CYSJ362A sensors mounted on the magnetic spring moved by the vibration generator, the LK-G152 and the LK-G32 Keyence laser heads, the function generator Signal Agilent Keysight 33120A, the Power Amplifier FPA2000-30W and the MDO3012 Tektronix MSO / MDO Oscilloscope as shown in Figure 4. The vibration generator was supplied by the function generator Signal Agilent Keysight 33120A and the achieved input voltage was amplified by the Power Amplifier FPA2000-30W generating the vibration motion of the rod in the vibration generator. For characterization of magnetic spring in order to achieve meaningful outcomes of displacement and magnetic flux density, the AC voltage signal varied in amplitudes of 1 V, 3 V,4 V and 5 V and in the frequency range from 0 Hz to 140 Hz. The input current and voltage were visualized on the MDO3012 Tektronix MSO / MDO Oscilloscope.

3.2 Measurement of the levitating magnet displacement in the magnetic spring

The measurement of the displacement in the magnetic spring were performed using LK-G3000 Keyence laser heads connected by driver LK-GD5000 with the PC supported by LK-Navigator program. In the LK-Navigator software program, the sampling cycle was set at 200 µs and the stored data were set to 60004 points. The laser distance sensor system uses laser triangulation

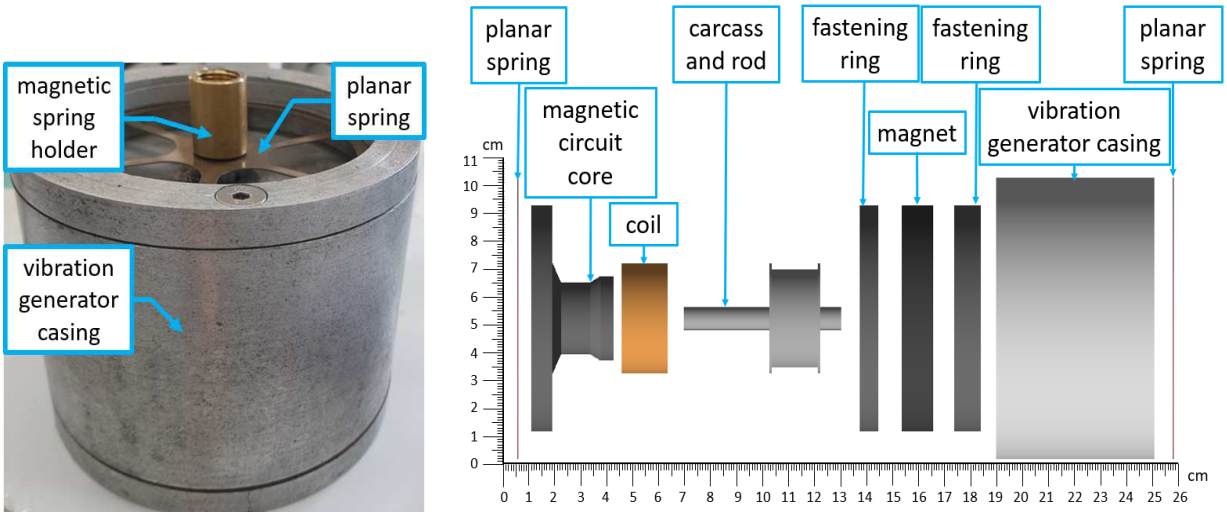

Fig. 3: (a) Realized Vibration Generator, (b) Structure of vibration generator

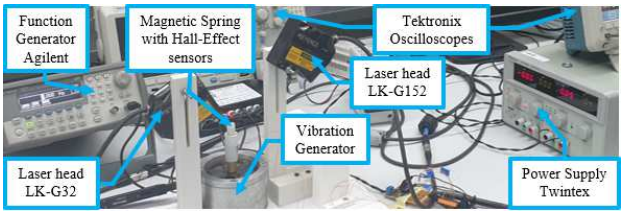

Fig. 4: Laboratory stand for the measurement of magnetic flux density: magnetic spring with Hall-Effect sensors supplied by Power Supply Twintex, the vibration generator supplied by the function generator signal Agilent Keysight 33120A with the Power Amplifier FPA2000-30W, MDO3012 Tektronix, MSO / MDO Oscilloscopes, the LK-G3000 Keyence laser heads and PC.

to calculate the distance via an angle measurement and the reflected light from the object depicted on the CCD ruler. The laser distance sensors LK-G32 with repeatability of 0.05 μm and LK-G152 with repeatability of 0.5 μm, were used respectively to measure the magnetic spring casing and the levitating magnet displacement relative to the surface support where the vibration generator is placed. The displacement of the levitating magnet relative to the magnetic spring is calculated as a function of the magnetic spring casing displacement and the levitating magnet displacement relative to the support base, given by Eq.5.

$$z_m = z_1 - z_2 \tag{5}$$

where z_m is the levitating magnet displacement relative to the magnetic spring, z_1 is the the levitating magnet displacement relative to the support base and z_2 is the magnetic spring casing. In Figure 5 the mentioned displacements are marked with blue color.

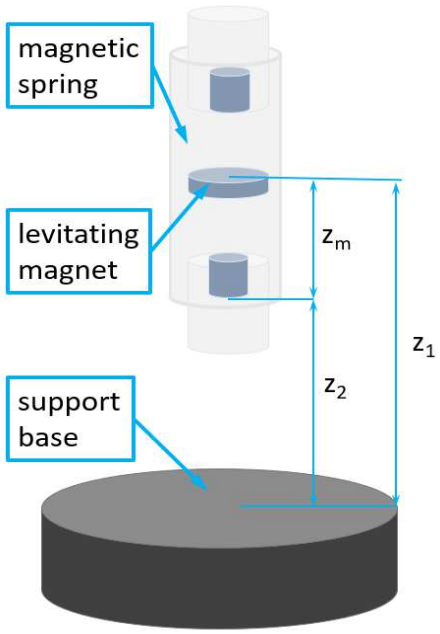

Fig. 5: Displacements of the levitating magnet and magnetic spring.

The amplitude of the levitating magnet displacement relative to the magnetic spring after the application of Fast Fourier Transform are shown in Figure 6.

The amplitude of the levitating magnet displacement is greater for the resonance frequencies (f_0) of the tested

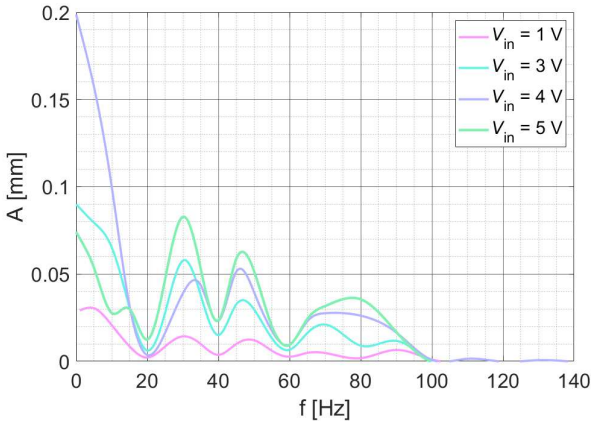

Fig. 6: Amplitude of the levitating magnet displacement in the magnetic spring as function of frequency obtained by LK-G3000 Keyence laser heads for external voltage of vibration generator of 1 V, 3 V, 4 V and 5 V.

system. Therefore the resonance frequencies of the magnetic spring (f_{m0}) are obtained corresponding to the amplitude of the displacement of the levitating magnet as shown in Figure 6. The resonance frequencies for the vibration generator f_{g0} are $\sim 2\ Hz$, 30 Hz, 50 Hz and 70 Hz.

In Figure 6, two additional f_0 corresponding to f_{m0} are visible at $\sim 85\ Hz$ and 110 Hz. The first f_{m0} equal to $\sim$85 Hz corresponds with the linear motion of the levitating magnet. The second f_{m0} equal to $\sim$ 110 Hz corresponds to the rotational motion of the levitating magnet. The lowest displacement of the levitating magnet in the magnetic spring is noticed for the vibration generator input voltage of 1 V, due to the low displacement of the vibration generator. The greatest displacement is observed for the input voltage of 5 V for the frequencies more than 20 Hz, due to high input power of the vibration generator $\sim 3\ W$. However, the greatest amplitude $\sim$ 0.2 mm for the 2 Hz is achieved for the input voltage of 4 V. For the input voltages of 4 V and 5 V the amplitudes of the levitating magnet displacement for the first f_{m0} equal to $\sim$ 85 Hz and for the f_{g0} equal to 70 Hz are indistinguishable, due to the great displacement of the vibration generator. Moreover, the f_{m0} equal to $\sim$ 110 Hz is the most visible for these input voltages, due to the great displacement of the vibration generator. For the operating input voltages of the vibration generator equal to 1 V and 3 V the levitating magnet mainly oscillates. Although, for the operating input voltages of the vibration generator equal to 4 V and 5 V the linear displacement of the levitating magnet appears more significant.

3.3 Measurements of magnetic flux density in the magnetic spring

The measurement of the magnetic flux density in the magnetic spring was carried out by the Hall-Effect CYSJ362A sensors made of mono-crystal gallium arsenide (GaAs) semiconductor material group III-V [36]. The parameters of the CYSJ362A Hall-Effect sensor are shown in Table 2. The Hall-Effect sensor measures the voltage fluctuation when the device is placed in a magnetic field. In the conducted tests, the sensors were supplied by 10 V voltage and 0.05 A current using the Power Supply Twintex TP-30102 Linear laboratory DC regulated 30V 10A Dual Channel Output power supply (Multichannel Power Supplies TWINTEX) and were connected in electric circuits with the capacitors of 4.7 μF and 100 nF (Figure 7 (a)) to enhance their performance.

Different measurements of magnetic flux density were carried out using the three Hall-Effect sensors located in upper, middle and bottom part of magnetic spring as shown in Figure 7 (b). In particular, for the upper and bottom magnets, the magnetic flux density was calculated in the perpendicular direction of the magnets height. Whereas, for the levitating magnet located in the middle of the magnetic spring, the magnetic flux density was calculated in the perpendicular direction of its radius.

In the measurement conducted by the Hall-effect sensors the output voltage, Hall Voltage V_H, is proportional to the magnetic flux density. The voltage signal obtained by the Hall-Effect sensors were displayed and measured by the MSO2024 Tektronix Mixed Signal Oscilloscope with the samples rate of 20 ms. The aforementioned output Hall voltage is obtained by equation:

$$V_H = V_{HM} - V_{OS}(V_u) \tag{6}$$

where V_H is the Hall Voltage in volts, V_{HM} is the measured voltage and V_{OS} is the offset voltage.

The measurements of the magnetic flux density in the magnetic spring were conducted for the input voltage of the Hall-effect sensors of 10 V, temperature of 20$^{\circ}C$, input voltage of the vibration generator 1 V, 3 V, 4 V and 5 V and for the frequency range from 0 Hz to 140 Hz. The dependency of magnetic flux density on Hall voltage B(V_H) can be obtained by technical specifications of the Hall-Effect CYSJ362A sensors in [36] and by the following equation:

$$B = 1/3.1333333 V_H \tag{7}$$

Therefore the Fast Fourier Transform was applied to output Hall voltage and the magnetic flux density was calculated by the Eq. 7 using the measured voltages detected by Hall-effect sensors.

The magnetic flux densities measured by the upper, middle and lower Hall-effect sensors in the magnetic spring as a function of frequency are displayed in Figure 8 (a), Figure 8 (b) and Figure 8 (c) respectively. As the

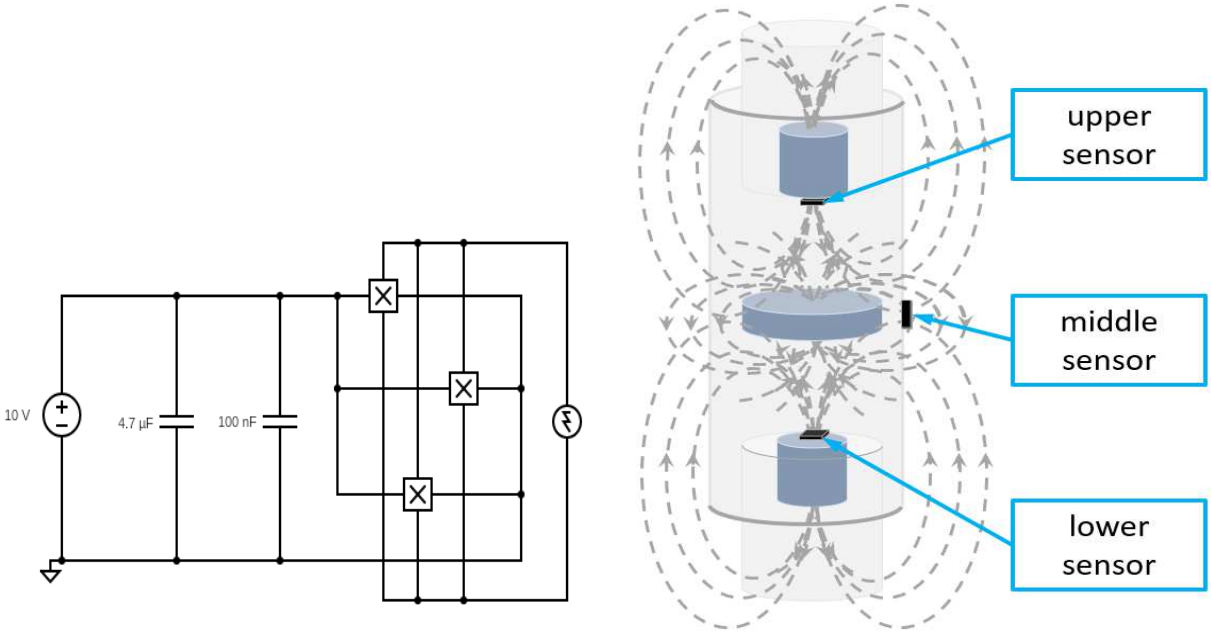

Fig. 7: (a) The circuit diagram of the Hall-Effect sensors connection (b) The Hall Effect Sensor placement

Table 2: Electrical characteristics and absolute maximum rating for CYSJ362A GaAs Hall- Effect Element [36]

Parameter	**Symbol**	**Value**	**Unit**	**Test conditions**
Hall output voltage	V_H	156∼204	mV	B=100 mT, V_C=6 V, Ta=25°C
Offset voltage	$V_{OS}(V_u)$	±8	mV	B=0 mT, V_C=6 V, Ta=25°C
Input resistance	R_{in}	1000∼1500	Ω	B=0 mT, Ic=0.1 mA, Ta=25°C
Output resistance	R_{out}	1800∼ 3000	Ω	B=0 mT, Ic=0.1 mA, Ta=25°C
Temperature coefficient of Hall output voltage	αV_H	-0.06	$\%/°C$	Ic=1 mA , B=100 mT (Ta=25°C ∼ 125°C)
Temperature coefficient of input resistance	αR_{in}	0.3	$\%/°C$	Ic=0.1mA, B=0mT (Ta=25 °C ∼ 125 °C)
Linearity	ΔK_H	2	%	B=0.1/0.5 T, Ic=1 mA, Ta=25°C
Max. Input Voltage	V_C	12V	V	–
Max. Input Power	P_D	150	mW	–
Operating temperature range	T_A	-40 ∼ 125	C	–
Storage temperature range	T_S	-55 ∼ 150	C	–
MTBF(Mean Time Between Failures)	–	>100k	hour	–

amplitude of the input voltage increases, the magnetic flux density, due to the greater displacement of the levitated magnet, rises.

In Figure 8 (a), Figure 8 (b) and Figure 8 (c) the displacement of the vibration generator for the input voltage of 1 V is too low to move the magnetic spring significantly, so the magnetic flux density is nearly 0 T. In the Figure 8 (b), for the very low frequency ∼ 2 Hz the magnetic flux density reaches the maximum value of ∼ 0.0152 mT, detected by the middle sensor. The input voltage greater than 1 V causes more visible displacement of the vibration generator and magnetic spring, and the increase of the magnetic flux density in correspondence of resonance frequencies of the vibration generator (2 Hz, 30 Hz, 50 Hz and 70 Hz) and the resonance frequencies magnetic spring (85 Hz and 110 Hz) for upper and middle sensor (Figure 8(a) and Figure 8(b)). For the non-resonance frequencies, the values of the magnetic flux density detected by the lower sensors in the magnetic spring (Figure 8(c)) are higher than detected by the upper and middle sensors. It is caused by the gravitational force acting on the levitating magnet. For input voltage ∼ 3 V the movement of the magnetic spring is low, so the levitating magnet mostly oscillates. Therefore the displacement of the levitated magnet is up to ∼ 0.2 mT for the second resonance frequency of the magnetic spring (110 Hz) associated with the rotational movement of the levitated magnet. For the input voltage of vibration

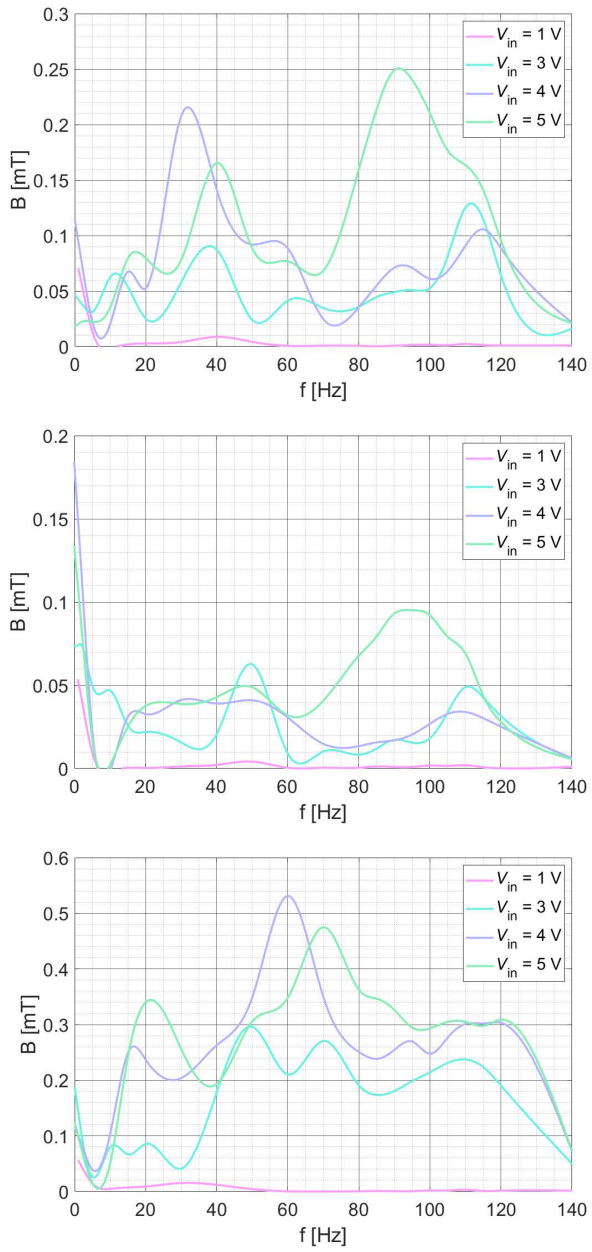

Fig. 8: Relative magnetic flux density of magnetic spring as function of frequency obtained by Hall-Effect sensors for external voltage of vibration generator that varies in the range from 1 V to 6 V: (a) for Hall-Effect sensor located on upper fixed magnet of magnetic spring ; (b) for Hall-Effect sensor located on levitated magnet of magnetic spring (c) for Hall-Effect sensor located on lower fixed magnet of magnetic spring.

generator equal 4 V two resonance frequencies 85 Hz and 110 Hz are achieved in correspondence of the high value of the magnetic flux density. For the input voltage of 5 V the value of the magnetic flux density for the first resonance frequency (85 Hz) of the magnetic spring is up to 0.5 mT and the second frequency is not noticeable. It is caused by high amplitude of the magnetic spring displacement and therefore higher linear displacement of the levitating magnet.

4 NARX EQUATION

The Artificial Neural Networks (ANNs) are computational models for solving many complex real-problem in clustering, recognition, pattern classification, optimization, function approximation and prediction. ANNs are mathematical algorithms and tools inspired by the biological human brain that perform dependencies between input and output information. The ANN networks are non-linear maps of m-dimensional input space onto an n-dimensional output space, when the mathematical relations between input and output variables contains unknown parameters. Generally, the ANN networks depend on the knowledge of the system to be modeled.

Considering that the magnetic flux density is a time series related to the nonlinear systems of magnetic spring and vibration generator, the NARX neural network is a good predictor of the time series that can be used in this research study. The nonlinear autoregressive network with exogenous inputs (NARX) model is a recurrent dynamic neural network that encloses several layers with feedback connections. NARX networks can be applied to nonlinear dynamic and time series models with much faster convergence and better generalization than other neural network models. To maximize the performance of the NARX neural network in nonlinear time series forecasting, it is considered its ”memory” ability to use the past values of the predicted or true time series. The mathematical expression for the output of NARX model is represented by the following equation:

$$\hat{y}(t) = f(y(t-1), y(t-2), ..., y(t-n_y), \\ u(t-1), u(t-2), ..., u(t-n_u)) + e(t) \quad (8)$$

where $y(t)$ is the target output variable, $\hat{y}(t)$ is the predicted output of the NARX model that is regressed on previous values of the output signal and previous values of the independent input signal, $u(t)$ is the input variable of the NARX, n_u is the number of input delays, n_y is the number of output delays, and $e(t)$ is the error value between the target and predicted values.

According to the input variable $u(t)$, the hidden layer output at time t is obtained as:

$$H_i(t) = f_1 \left[\sum_{r=0}^{n_u} w_{ir} u(t-r) + \sum_{l=1}^{n_y} w_{il} y(t-l) + a_i \right] \quad (9)$$

where w_{ir} is the connection weight between the input neuron $u(t-r)$ and i_{th} hidden neuron, w_{il} is the

connection weight between the i_{th} hidden neuron and the output feedback $y(t-l)$, a_i is the bias of the i_{th} hidden neuron and f_1 is the hidden layer activation function. The final prediction equation can be expressed as a combination of Eq.8 and Eq. 9.

$$\hat{y}_j(t) = f_2\left[\sum_{i=1}^{n_h} w_{ji}H_i(t) + b_j\right] \tag{10}$$

where f_2 is the output layer activation function with an argument being a sum of a bias of a j_{th} predicted output b_j plus a weighted sum of the hidden layer outputs $H_i(t)$ taken with weights w_{ji}, calculated for n_h hidden neurons as in [37].

In this work, the MATLAB Neural Network tool has been used to build the NARX models for a combination of the magnetic flux density time-series data sets and the geometry of the magnetic spring, the input voltages of the vibration generator, input voltages frequencies and displacement of the levitated magnet in the magnetic spring as shown in Figure 9. Not only the relation between the inputs (geometry of the magnetic spring, input voltages of the vibration generator, input voltages frequencies and movement of the levitated magnet) and the desired output of magnetic flux density in the magnetic spring is provided by the neural network, but also the prediction of the output variables value of magnetic flux density in future instants of time. In fact, the investigated magnetic spring system is affected by the nonlinear vibrations in the frequency domain generated by the vibration generator. Also the dynamic and complexity provided by the non-linearity can be seen in the levitated magnet displacement that impacts the analyzed magnetic flux density in the magnetic spring. The proposed theoretical model based on NARX networks can be adapted to describe the physical magnetic phenomena and the characterization of the strong non-linearity involved in the measurements of the magnetic spring to achieve the optimum results and improve the modelling of the prototype. The NARX network model for magnetic spring can be expressed as:

$$\hat{B}(t) = f[x(t), f, V, h, V_{in}, B(t-1), ..., B(t-n_B))] \tag{11}$$

where $\hat{B}(t)$ is the predicted value of magnetic flux density, $x(t)$ is the displacement of the levitated magnet in the magnetic, f is the input voltages frequency, V is the volume of the fixed magnet and levitated magnet, h is the height of the fixed magnet and levitated magnet in the magnetic spring, V_{in} is the input voltage of vibration generator, $B(t)$ is the magnetic flux density measured by Hall-Effect sensors, and $n_B = 1$ is the time delay.

The architectures of a NARX network consist of three different layers: input, which includes the input parameters of the network, hidden layer, and output layer. The Matlab Code was used to automatically normalize input and target data and un-normalize output results. The neural network is trained and initialised with a set of weights. These weights are then optimised during the training period and the optimum weights are obtained. The bias is a constant parameter-vector added to the product of inputs and weights utilised to offset the result. For the modeling a set of 5 input variables, three hidden layer and the output variable were considered. The input variables training data selected for the developed NARX model are the input voltage of vibration generator of 1 V, 3 V, 4 V and 5 V and the input voltage frequency from 0 to 140 Hz, the geometry including volume and height of fixed magnets and levitating magnet, and mean value of levitating magnet displacement as shown in the Figure 9. The output variable is the magnetic flux density obtained by Hall-sensor effect measurement for the two fixed magnet and the levitated magnet of magnetic spring. The magnetic flux density of magnetic spring in function of frequency is obtained by Hall-Effect sensors located at the corresponding fixed magnets (in upper and lower position) and floating magnet (middle position) for external voltage of vibration generator that varies from 1 V to 6 V. In the developed neural network, the first and second hidden layer contain 7 number of neurons with respectively log-sigmoid transfer function called Logsig ($f(n) = logsig(n) = 1/(1+exp(-n))$) and Hyperbolic tangent sigmoid transfer function called also Tansig ($f(n) = tansig(n) = 2/(1+exp(-2*n)) - 1$), the third hidden layer only 6 neurons with tansig transfer function and a linear transfer function for the output layer as shown in Figure 10. The network training function Bayesian regularization, trainbr, that updates the weight and bias values according to Levenberg-Marquardt optimization has been implemented in training neural network.

It determines the minimization of the appropriate combination of the squared error and weights for network generalization. The best validation performance for Mean Square Error (MSE) is 6.1132e-9 at 998 epochs as shown in Figure 11.

After the accurate training, learning and validation process, the weights parameters associated to hidden layer 1 from input 1 are shown in the Table 3, the weights parameters associated to hidden layer 2 from hidden layer 1 are shown in the Table 4, the weights parameters associated to hidden layer 3 from hidden layer 2 in the Table 5, the weights associated to hidden layer 4 (or Output layer) from hidden layer 2 in the Table 6, and the weights associated to hidden layer 1 from hidden layer 4 (or Output layer) in the Table 7. The biases parameters associated to the layers are shown in the Table 8 and in the Table 9. The final mathematical relation of magnetic flux density prediction as function of frequency, magnetic spring's geometry, vibration generator's input voltage, and displacement of levitated magnet in magnetic spring is expressed as a combination of Eq.10 and Eq.11 with the weights and bias parameters obtained by computational neural model.

The Figure 12(a), Figure 12(b), Figure 12(c) represent the results of the developed Narx model of the prediction

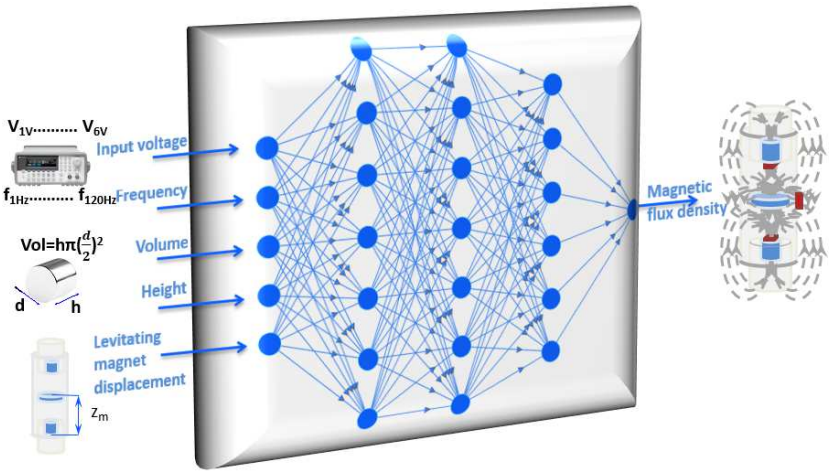

Fig. 9: Developed NARX with inputs and output.

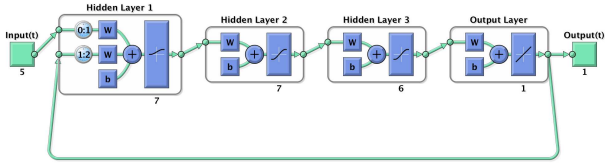

Fig. 10: View design of structure neural network.

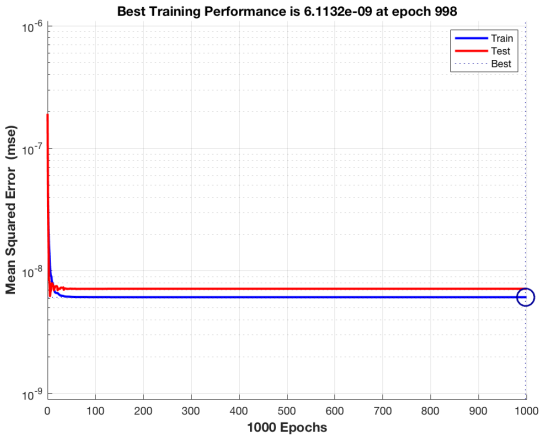

Fig. 11: Training Performance of neural network

Table 3: Weight to hidden layer 1 from input 1

i/j	1	2	3	...	10
1	0.071042	0.099864	-0.22672	...	0.00044682
2	0.11454	-0.029476	-0.33076	...	-0.00089211
...	...	...	...	...	...
7	1.9005	-1.2134	0.15919	...	-0.0039798

Table 4: Weight to hidden layer 2 from hidden layer 1

i/j	1	2	3	...	7
1	-0.27228	-0.20086	0.081792	...	0.87682
2	0.052804	0.066778	-0.15028	...	-0.3711
...	...	...	...	...	...
7	0.052804	-0.066778	0.15028	...	0.3711

Table 5: Weight to hidden layer 3 from hidden layer 2

i/j	1	2	3	...	7
1	0.30256	-0.052127	-0.29461	...	0.052127
2	0.30256	-0.052127	-0.29461	...	0.052127
...	...	...	...	...	...
6	0.30256	-0.052127	-0.29461	...	0.052127

Table 6: Weight to hidden layer 4 (or Output layer) from hidden layer 2

i/j	1	2	3	...	6
1	0.51983	0.51983	0.51982	...	0.51983

of magnetic flux density of magnetic spring in function of frequency.

The Figure 12(a) shows the results of the magnetic flux density prediction obtained by neural network and the magnetic flux density achieved by Hall-Effect sensor located at the upper fixed magnet for external voltage of vibration generator that varies from 1 V to 6 V. The RMSE (Root Mean Square Error) between the original and predicted magnetic flux density obtained by upper sensor in magnetic spring is equal 0.1935.

The Figure 12(b) shows the results of prediction of magnetic flux density obtained by neural network and the

Table 7: Weight to hidden layer 1 from hidden layer 4 (Output layer)

i/j	1	2
1	1.3049e-172	2.6838e-172
2	1.4012e-172	1.4336e-172
...	...	...
7	2.3239e-174	-3.8244e-172

Table 8: Bias to layer 1 and Bias to layer 2

	1	2	...	7
b(1)	0.00119	-0.0023759	...	-0.010599
b(2)	-0.25068	0.023375	...	-0.023375

Table 9: Bias to layer 3

	1	2	...	6
b(3)	0.074165	0.074165	...	0.074165

magnetic flux density achieved by Hall-Effect sensor located at the middle levitated magnet for external voltage of vibration generator that varies from 1 V to 6 V. The RMSE between the original and predicted magnetic flux density obtained by middle sensor in magnetic spring is equal 0.0682.

The Figure 12(c) shows the results of prediction of magnetic flux density obtained by neural network and the magnetic flux density achieved by Hall-Effect sensor located at the lower fixed magnet for external voltage of vibration generator that varies from 1 V to 6 V. The RMSE between the original and predicted magnetic flux density for the lower sensor in magnetic spring is equal 0.1693.

The prediction performance of magnetic flux density by NARX is more accurate for the levitated magnet in magnetic spring as observed in Figure 12(b) because the proposed external input data are focused mainly on information (geometry and displacement) of the levitated magnet in the magnetic spring. It is possible to view the resonance frequencies of magnetic spring for 6 V voltage of both predicted and original magnetic flux density in Figure 12(b). In Figure 12(b) and Figure 12(c) for the external voltage less of 2 V, the NARX neural network accurately predicted the magnetic flux density because the vibration generator movement is not so strong and the levitated magnet displacement is more significant than the vibration generator displacement for the resonance frequencies of magnetic spring.
In the Fig.12 the accuracy of the predicted model is low for estimation of amplitude of the magnetic flux density in the frequency range from 1 to 140 Hz with absolute error of 50 %, due to the high non-linearity of the system. However the computed absolute error of 20% and 10 % of predicted magnetic flux density is obtained respectively for frequency of 50 Hz and 90 Hz and voltage of 4 V, 5 V and 6 V useful for the energy harvesting system.

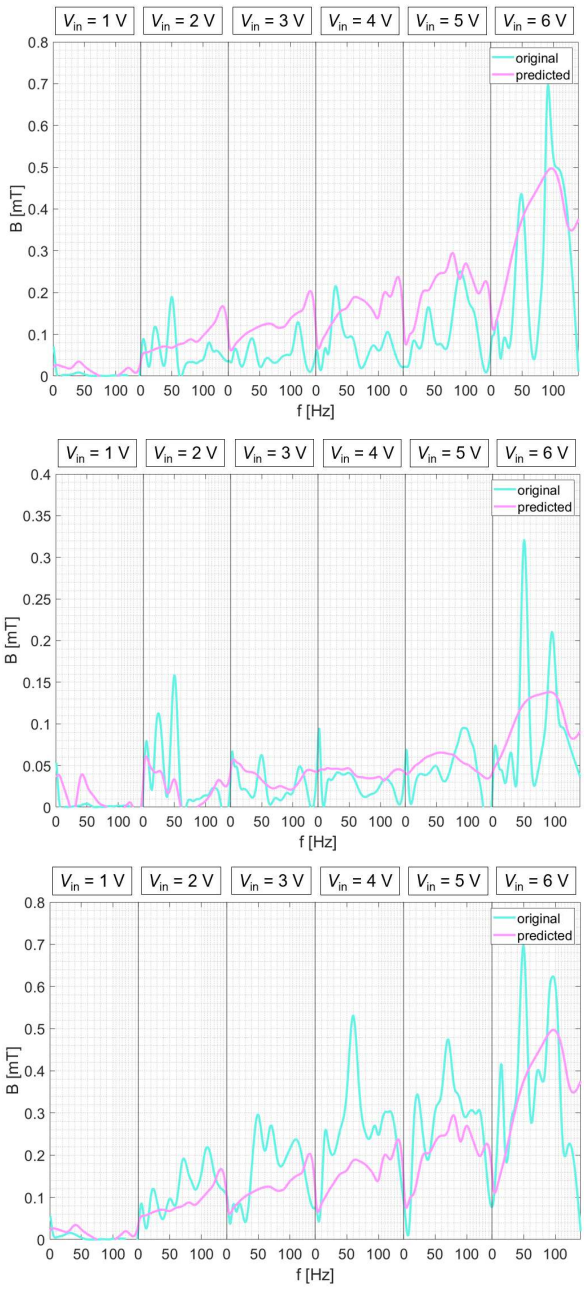

Fig. 12: Relative magnetic flux density of magnetic spring as function of frequency predicted and obtained by the Hall-Effect sensors: (a) for Hall-Effect sensor located on upper fixed magnet of magnetic spring ; (b) for Hall-Effect sensor located on levitated magnet of magnetic spring (c) for Hall-Effect sensor located on lower fixed magnet of magnetic spring

5 Conclusion

This article investigates the mechanical and magnetic properties of a realized prototype consisting of the

magnetic spring located on the vibration generator in the vertical position. The levitating permanent magnet and two identical fixed magnets enclosed in the polyamide casing are included in the magnetic spring. The motion of the magnetic spring is generated by the vibration generator causing the displacement of the levitating magnet and the change in the magnetic flux density.
The experimental test measurements of the levitating magnet displacement have been conducted in the laboratory using function generator, power amplifier, oscilloscope and laser distance meters. The magnetic flux density values in the magnetic spring have been detected by the three Hall-Effect sensors mounted on the magnetic spring.
The magnetic spring is excited by the designed vibration generator that generates the nonlinear vibrations in the frequency domain. The conducted analysis was focused on the non-linearity and complexity exhibited by the displacement of the levitating magnet that affect the magnetic flux density in the magnetic spring. The nonlinear phenomena of the magnetic spring has been exploited using as a solution the nonlinear autoregressive network with exogenous inputs (NARX) model that captures the dynamic of the magnetic spring system. For this purpose, the relation between the inputs data corresponding values of geometrical parameters of the magnetic spring, input voltage of vibration generator, input voltages frequency, displacement of the levitating magnet and the output data corresponding the magnetic flux density has been described by the NARX model. The predicted magnetic flux density were validated with the available experimental data set. In the case of the magnetic flux density obtained by upper, middle and lower sensors in the magnetic spring, the deviation between simulated and measured values is acceptable with the RMSE equal 0.1935, 0.0682 and 0.1693 respectively. The NARX model has provided a mathematical relationship between the magnetic flux densities and parameters with high non-linearity and complexity, although the accuracy of the predictive model is not high. The limitation of this work is due to the high complexity and non-linearity causes by vibrations, displacements and frequency within the energy harvesting system. The representative relation-algorithm based on the NARX equation could be a valid approach in the future manufactured design of the magnetic spring and a potential solution to enhance the harvested electric power for engineering applications. However the predicted results of NARX show most an effective qualitative analysis exhibiting low values of resonances frequencies especially for the lower sensor. To obtain a detailed prediction result various methods and approaches will be proposed and investigated in the future works.

Ethical approval:

This article does not contain any studies with human participants performed by the author.

Acknowledgments

The authors are thankful to the Deanship of Graduate Studies and Scientific Research at University of Bisha for supporting this work through the Fast-Track Research Support Program.

Data Availability Statement

Data sharing is not applicable to this article as no data sets were generated during the current study.

Conflicts of Interest

The authors declare that there is no conflicts regarding the publication of this paper.

References

[1] A. Harb, Energy harvesting: State-of-the-art, *Renewable Energy* **36**(10) (2011) 2641–2654.
[2] S. Bai and C. Liu, Overview of energy harvesting and emission reduction technologies in hybrid electric vehicles, *Renewable and Sustainable Energy Reviews* **147** (2021) p. 111188.
[3] H. Pan, L. Qi, Z. Zhang and J. Yan, Kinetic energy harvesting technologies for applications in land transportation: A comprehensive review, *Applied Energy* **286** (2021) p. 116518.
[4] N. Wu, B. Bao and Q. Wang, Review on engineering structural designs for efficient piezoelectric energy harvesting to obtain high power output, *Engineering Structures* **235** (2021) p. 112068.
[5] N. Tran, M. H. Ghayesh and M. Arjomandi, Ambient vibration energy harvesters: A review on nonlinear techniques for performance enhancement, *International Journal of Engineering Science* **127** (2018) 162–185.
[6] M. A. Abdelkareem, L. Xu, M. K. A. Ali, A. Elagouz, J. Mi, S. Guo, Y. Liu and L. Zuo, Vibration energy harvesting in automotive suspension system: A detailed review, *Applied energy* **229** (2018) 672–699.
[7] C. Saha, T. O'donnell, N. Wang and P. McCloskey, Electromagnetic generator for harvesting energy from human motion, *Sensors and Actuators A: Physical* **147**(1) (2008) 248–253.
[8] S. Khalid, I. Raouf, A. Khan, N. Kim and H. S. Kim, A review of human-powered energy harvesting for smart electronics: recent progress and challenges, *International Journal of Precision Engineering and Manufacturing-Green Technology* **6** (2019) 821–851.

[9] C. Wei and X. Jing, A comprehensive review on vibration energy harvesting: Modelling and realization, *Renewable and Sustainable Energy Reviews* **74** (2017) 1–18.
[10] B. Maamer, A. Boughamoura, A. M. F. El-Bab, L. A. Francis and F. Tounsi, A review on design improvements and techniques for mechanical energy harvesting using piezoelectric and electromagnetic schemes, *Energy Conversion and Management* **199** (2019) p. 111973.
[11] Y. Peng, L. Zhang, Z. Li, S. Zhong, Y. Liu, S. Xie and J. Luo, Influences of wire diameters on output power in electromagnetic energy harvester, *International Journal of Precision Engineering and Manufacturing-Green Technology* (2022) 1–12.
[12] A. E. ELGebaly and M. K. El-Nemr, Optimized design of pm halbach array linear generator for sea wave energy converters operate at maximum power transfer, *Advances in Science, Technology and Engineering Systems* **4**(4) (2019) 440–448.
[13] Z. Liu, X. Wang, E. Al Shami, N. J. Baker and X. Ji, A study of a speed amplified linear generator for low-frequency wave energy conversion, *Mechanical Systems and Signal Processing* **149** (2021) p. 107226.
[14] J. Yunas, N. Indah, H. M. Hanifah, I. Hamidah, D. F. Ramadhan, I. Mustagisin, B. Bais and A. A. Hamzah, Mechanical charaterization of mems vibration membrane with planar spring design for energy harvester, *J. Eng. Sci. Technol* **15**(5) (2020) 3178–3188.
[15] P. Carneiro, M. P. S. dos Santos, A. Rodrigues, J. A. Ferreira, J. A. Simões, A. T. Marques and A. L. Kholkin, Electromagnetic energy harvesting using magnetic levitation architectures: A review, *Applied Energy* **260** (2020) p. 114191.
[16] M. L. Monaco, C. Russo and A. Somá, Numerical and experimental performance study of two-degrees-of-freedom electromagnetic energy harvesters, *Energy Conversion and Management: X* (2023) p. 100348.
[17] Z. Li, Y. Liu, P. Yin, Y. Peng, J. Luo, S. Xie and H. Pu, Constituting abrupt magnetic flux density change for power density improvement in electromagnetic energy harvesting, *International Journal of Mechanical Sciences* **198** (2021) p. 106363.
[18] Z. Li, Z. Yan, J. Luo and Z. Yang, Performance comparison of electromagnetic energy harvesters based on magnet arrays of alternating polarity and configuration, *Energy conversion and management* **179** (2019) 132–140.
[19] J. Bijak, T. Trawiński, M. Szczygieł and Z. Kowalik, Modelling and investigation of energy harvesting system utilizing magnetically levitated permanent magnet, *Sensors* **22**(17) (2022) p. 6384.
[20] J. Bijak, G. Lo Sciuto, Z. Kowalik, T. Trawiński and M. Szczygieł, A 2-dof kinematic chain analysis of a magnetic spring excited by vibration generator based on a neural network design for energy harvesting applications, *Inventions* **8**(1) (2023) p. 34.
[21] H. Liao, T. Ye, Y. Pang, C. Feeney, L. Liu, Z. Zhang, C. Saha and N. Wang, Modelling and optimization of a magnetic spring based electromagnetic vibration energy harvester, *Journal of Electrical Engineering & Technology* (2022) 1–12.
[22] M. Hasani and M. I. Rahaghi, The optimization of an electromagnetic vibration energy harvester based on developed electromagnetic damping models, *Energy Conversion and Management* **254** (2022) p. 115271.
[23] H. Wu, Y. Zhang, W. Fu, C. Zhang and S. Niu, A novel pre-processing method for neural network-based magnetic field approximation, *IEEE Transactions on Magnetics* **57**(10) (2021) 1–9.
[24] M. Le, C.-T. Pham and J. Lee, Deep neural network for simulation of magnetic flux leakage testing, *Measurement* **170** (2021) p. 108726.
[25] C. Xu, C. Wang, F. Ji and X. Yuan, Finite-element neural network-based solving 3-d differential equations in mfl, *IEEE Transactions on Magnetics* **48**(12) (2012) 4747–4756.
[26] I. Marinova, C. Panchev and D. Katsakos, A neural network inversion approach to electromagnetic device design, *IEEE transactions on magnetics* **36**(4) (2000) 1080–1084.
[27] D. Shi, E. Šabanovič, L. Rizzetto, V. Skrickij, R. Oliverio, N. Kaviani, Y. Ye, G. Bureika, S. Ricci and M. Hecht, Deep learning based virtual point tracking for real-time target-less dynamic displacement measurement in railway applications, *Mechanical Systems and Signal Processing* **166** (2022) p. 108482.
[28] J. Liu and X. Yang, Artificial neural network for vibration frequency measurement using kinect v2, *Shock and Vibration* **2019** (2019).
[29] S. Bagheri, N. Wu and S. Filizadeh, Application of artificial intelligence and evolutionary algorithms in simulation-based optimal design of a piezoelectric energy harvester, *Smart Materials and Structures* **29**(10) (2020) p. 105004.
[30] P. Mangaiyarkarasi, P. Lakshmi and V. Sasrika, Enhancement of vibration based piezoelectric energy harvester using hybrid optimization techniques, *Microsystem Technologies* **25** (2019) 3791–3800.
[31] R. Rath, D. Dutta, R. Kamesh, M. H. Sharqawy, S. Moulik and A. Roy, Rational design of high power density "blue energy harvester" pressure retarded osmosis (pro) membranes using artificial intelligence-based modeling and optimization, *Energy Conversion and Management* **253** (2022) p. 115160.
[32] S. Pathak, R. Zhang, K. Bun, H. Zhang, B. Gayen and X. Wang, Development of a novel wind to electrical energy converter of passive ferrofluid levitation through its parameter modelling and optimization, *Sustainable Energy Technologies and Assessments* **48** (2021) p. 101641.
[33] G. L. Sciuto, J. Bijak, Z. Kowalik, P. Kowol, R. Brociek and G. Capizzi, Deep learning model for magnetic flux density prediction in magnetic spring on the vibration generator, *IEEE Access* (2024).
[34] J. Bijak, G. L. Sciuto, Z. Kowalik, P. Lasek, M. Szczygieł and T. Trawiński, Magnetic flux density analysis of magnetic spring in energy harvester by hall-effect sensors and 2d magnetostatic fe model, *Journal of Magnetism and Magnetic Materials* (2023) p. 170796.
[35] W. Robertson, B. Cazzolato and A. Zander, A simplified force equation for coaxial cylindrical magnets and thin coils, *IEEE Transactions on magnetics* **47**(8) (2011) 2045–2049.
[36] Hall-effect element hall-effect element http://www.hallsensors.de/CYSJ362A.pdf, Accessed: 2023.
[37] Q. Liu, W. Chen, H. Hu, Q. Zhu and Z. Xie, An optimal narx neural network identification model for a magnetorheological damper with force-distortion behavior, *Frontiers in Materials* **7** (2020) p. 10.